

PHYSICOCHEMICAL ANALYSIS
OF INORGANIC SYSTEMS

Sm–Sm₂Se₃ Phase Diagram and Properties of Phases

N. Yu. Fainberg^a, O. V. Andreev^a, V. B. Kharitontsev^b, and A. A. Polkovnikov^b

^aTyumen State University of Oil and Gas, ul. Perekopskaya 15a, Tyumen, 625008 Russia

^bTyumen State University, Tyumen, ul. Semakova 10, Tyumen, 625003 Russia

e-mail: o.v.andreev@utmn.ru

Received January 27, 2015

Abstract—A Sm–Sm₂Se₃ phase diagram has been studied from 1000 K until melting. This system forms three congruently melting compounds: SmSe (ST NaCl, $a = 0.6200$ nm, $T_m = (2400 \pm 50)$ K, and $H = 2750$ MPa), Sm₃Se₄ (ST Th₃P₄, $a = 0.8925$ nm, $T_m = (2250 \pm 30)$ K, and $H = 3350$ MPa), and Sm₂Se₃ (ST Th₃P₄, $a = 0.8815$ nm, $T_m = (2150 \pm 40)$ K, and $H = 5300$ MPa). There are eutectics between Sm and SmSe phases and between SmSe and Sm₃Se₄ phases at 2.5 at % Se, 1300 K and at 54.5 at % Se, 2100 K, respectively. Within the extent of Sm²⁺Sm₂³⁺Se₄–Sm₂³⁺Se₃ solid solution (ST Th₃P₄), the experimentally determined percentages of Sm²⁺ ions correspond with the values calculated from the formula compositions of samples. The bandgap width for SmSe_{1.45} and SmSe_{1.48} phases is $\Delta E = (1.90 \pm 0.05)$ eV.

DOI: 10.1134/S0036023616010095

Samarium with selenium forms the compounds SmSe (ST NaCl, $a = 0.6200$ nm) and Sm₃Se₄ (ST Th₃P₄, $a = 0.8925$ nm) [1]. The low-temperature phase α -Sm₂Se₃ has an orthorhombic Sb₂S₃-type structure with $a = 1.127$ nm, $b = 0.409$ nm, $c = 1.095$ nm [2–4]; the high-temperature phase γ -Sm₂Se₃ has an orthorhombic structure (ST Th₃P₄, $a = 0.8875$ nm) [1–5]. The polymorphic transition from α -Sm₂Se₃ to γ -Sm₂Se₃ occurs at 1270 K; $\Delta H = 710$ J/mol [5]. The Sm₂Se₃ melting temperature was calculated to be 1810°C [1].

Samarium polyselenides (monoclinic Sm₄Se₇ and tetragonal SmSe_{1.8}) thermally dissociate at high temperatures to lose some selenium [1]. Pressure measurement is the major tool to study rare-earth chalcogenides [6].

The SmSe phase, which has conductivity $\rho = 2 \times 10^3 \Omega \text{ cm}$ and charge carrier concentration $n = 10^{15} \text{ cm}^{-3}$, was used as a thermoresistor. From the value of effective magnetic moment $\mu_{\text{eff}} = 2.18 \mu_B$, we inferred that there are two Sm³⁺ ions and one Sm²⁺ ion per Sm₃Se₄ formula unit [1].

Neither the melting temperature nor melting character has been earlier determined for SmSe, Sm₃Se₄, and Sm₂Se₃ [1–18].

Constructing a SmS–Sm₂S₃ diagram will help to choose methods and protocols for preparing samples of samarium selenides SmSe, Sm₃Se₄, and Sm₂Se₃ which are materials of applied importance.

This study is targeted at constructing a SmSe–Sm₂Se₃ phase diagram and determining the valence states of samarium and the properties of phases in the range Sm₃Se₄–Sm₂Se₃.

EXPERIMENTAL

Samples were prepared from metallic samarium (CmM-1 type) and selenium (high-purity grade 22-4). Samarium and selenium weights taken in set proportions, the total weight being 5 g, were placed in a silica ampoule of 10–15 mL in capacity; the ampoule was degassed and sealed off and then heat treated in a muffle. Starting with 570 K, the temperature was elevated by 50 K each 24 h until it reached 1270 K, and then maintained at this level for 100 h [3, 4, 9]. In order to prepare a Sm₂Se₃ sample, up to 0.5% excessive selenium was placed into an ampoule to evolve to the gas phase during heat treatment at 1270 K [3].

An as-synthesized sample was pounded and fused by high-frequency currents in a tantalum (50–54 at % Se) or a graphite (56–60 at % Se) crucible. The sample was twice melted and then cooled. A 60 at % Se sample was heat treated in selenium vapor [7, 8]. Samples were annealed for 15 min at (1750–1770) K. The temperature maintenance accuracy is ± 10 K in muffle furnaces and ± 30 K in high frequency currents setup [3–9].

The onset melting temperatures and complete melting temperatures of samples were determined by visual polythermal analysis (VPTA) [7, 10]. SmSe, Sm₃Se₄, and Sm₂Se₃ samples melted at temperatures

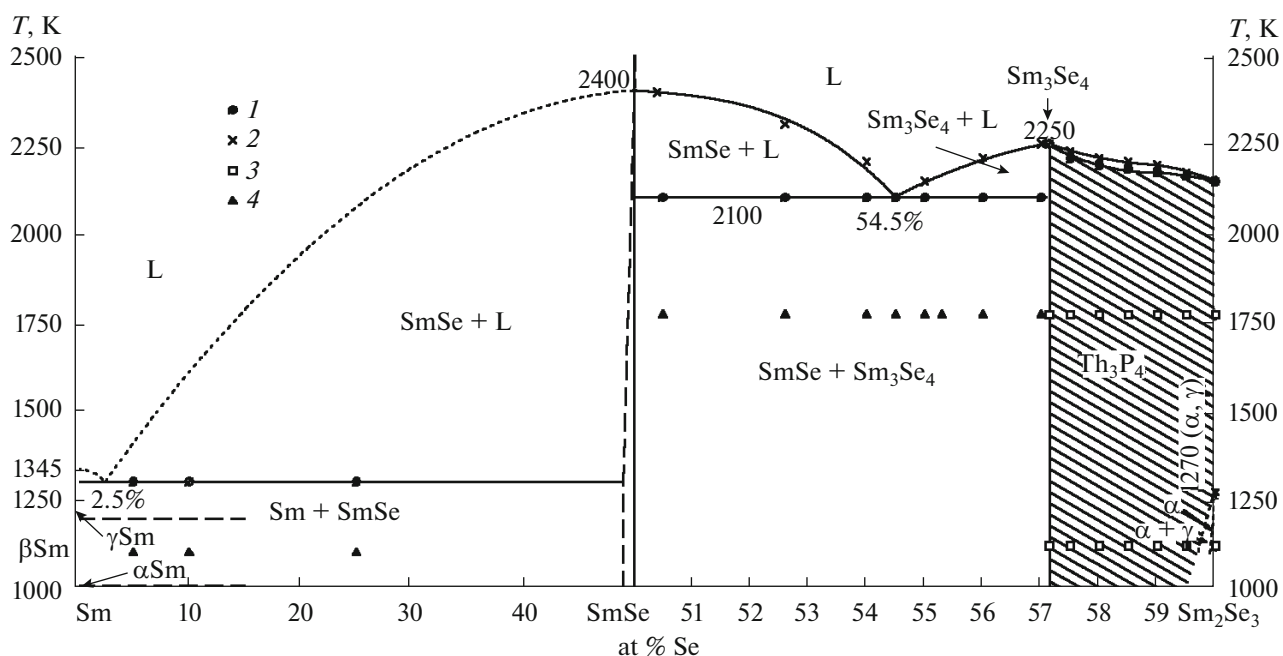


Fig. 1. Sm–Sm₂Se₃ phase diagram. The state of samples as probed by VPTA: (1) onset melting and (2) complete melting. The state of samples as probed by X-ray powder diffraction and microstructure observation: (3) single-phase and (4) two-phase constitution.

in the range 20–40 K on the average. The temperature at which a sample was rapidly shrunk was taken to be the melting temperature of the sample. Temperature determination accuracy was from ± 30 to ± 50 K and each time is indicated in the text.

X-ray powder diffraction (XRD) experiments were performed on a Dron-7 diffractometer (Ni-filtered $\text{CuK}\alpha$ radiation). Unit cell parameter determination accuracy was ± 0.0002 nm for cubic phases and ± 0.001 nm for orthorhombic phases.

Microstructure observation (MSA) was performed on an MeTAM LV-31 optical microscope in reflected light. Microhardness was measured with a PTM-3M tester with precision of 5 to 7%. The methods used to determine samarium valence states and optical characteristics of samarium selenides are described earlier [8].

RESULTS AND DISCUSSION

The Sm–Sm₂Se₃ system forms three congruently melting compounds: SmSe, Sm₃Se₄, and Sm₂Se₃ (Fig. 1). Eutectics are formed between Sm and SmSe and between SmSe and Sm₃Se₄. At temperatures above 1300 K, a solid solution having Th₃P₄-type cubic structure (a γ -phase) exists over the range Sm₃Se₄–Sm₂Se₃.

The phase compositions of 50 at % Se samples (SmSe phase) depends on the temperature schedule of high-temperature treatment. As-synthesized samples were cast allows once treated at 2350–2450 K and

were comprised of two phases as probed by XRD and MSA. Phase percentages are as follows: SmSe (ST NaCl, $a = 0.6200$ nm) > 95 mol %; Sm₃Se₄ (ST Th₃P₄, $a = 0.8925$ nm) < 5 mol %. Polished sections of ingots show SmSe faceted grains with angles of 120°. Sm₃Se₄ grains appear as strips in between SmSe grains (Fig. 2). The treatment of as-synthesized samples at 1900–2000 K yielded single-phase SmSe ($a = 0.6200$ nm) cakes; average microhardness of SmSe grains is $H = 2750$ MPa (Fig. 3). Samarium monoselenide, just as the SmS phase [11, 12], dissociated during heat treatment by the reaction



Plaque formed in the cooler parts of the reactor was identified as metallic samarium.

No extensive SmSe-base solid solutions were found [11]. In a 49.5 at % Se sintered sample, metallic samarium was observed in between SmSe grains, in a 50.5 at % Se sintered sample, a Sm₃Se₄ ($a = 0.8925$ nm) phase was found in between SmSe grains.

The congruent melting temperature of the SmSe phase is 2400 ± 50 K as determined by VPTA. The congruent melting of SmSe was inferred from the liquidus position. There is a peak at the SmSe line. The SmSe phase forms eutectics with the conjugated phases of metallic samarium and the Sm₃Se₄ phase.

The samples of Sm₃Se₄ phase prepared in sinters or fused cooled into single phases. X-ray diffraction patterns of these samples feature only reflections from the

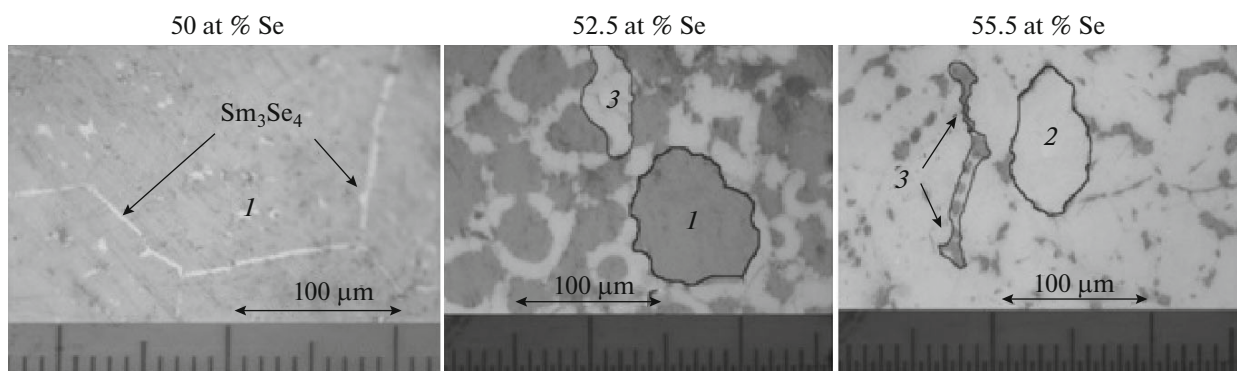


Fig. 2. Micrographs of SmSe–Sm₂Se₃ samples. These samples were prepared by melt solidification. Phases: (1) SmSe, (2) Sm₃Se₄, and (3) eutectic between SmSe and Sm₃Se₄ phases containing 54.5 at % Se.

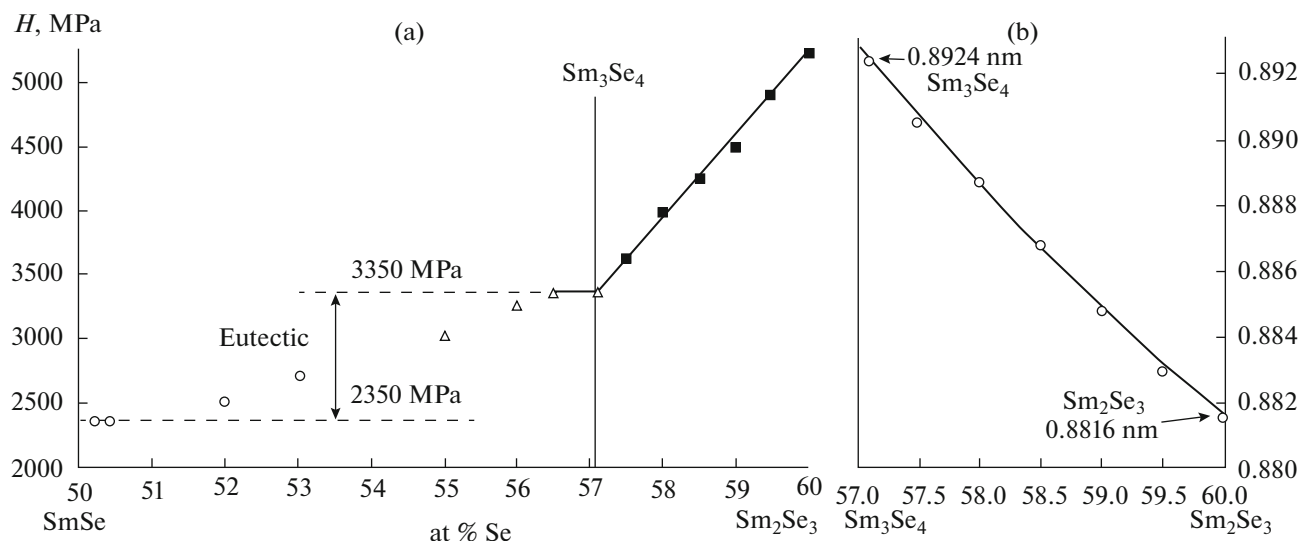


Fig. 3. Panel (a): microhardness versus composition plot for SmSe–Sm₂Se₃ samples annealed at 1770 K. Microhardness values: for SmSe, 2350 MPa (load $P=0.05$ kg); for Sm₃Se₄, 3350 MPa ($P=0.05$ kg); and for Sm₂Se₃, 5300 MPa ($P=0.05$ kg). Panel (b): unit cell parameter for a Th₃P₄-type cubic structure versus composition in the region of Sm₃Se₄–Sm₂Se₃ continuous solid solution.

Sm₃Se₄ phase (ST Th₃P₄, $a = 0.8925$ nm). The grain sizes as assessed by MSA averages 50–100 μm ; microhardness $H = 3350$ MPa. The congruent melting temperature of the Sm₃Se₄ phase as determined by VPTA is 2250 ± 30 K.

As-synthesized samples of Sm₂Se₃ phase were loose cakes. These samples were single phases according to XRD; their diffraction patterns features only reflections from an α -Sm₂Se₃ phase, a Sb₂S₃-type orthorhombic structure ($a = 1.127$ nm, $b = 0.409$ nm, $c = 1.095$ nm, unit cell volume $V = 5.041$ nm³).

The Sm₂Se₃ samples were annealed and fused under a selenium vapor atmosphere. A single-phase γ -Sm₂Se₃ sample ($a = 0.8816$ nm) was obtained. Microstructure observation of an etched polished section (HCl 1 : 150) showed oval grains with sizes of 50–80 μm having microhardness of 5300 MPa. The

Sm₂Se₃ phase melts congruently. The phase composition of the sample remained unchanged in the melting–cooling process. The Sm₂Se₃ melting temperature was 2150 ± 40 K.

A continuous solid solution having Th₃P₄ type structure $[(\text{Sm}_{(8-2x)/3}^{3+}(\text{Sm}^{2+})_x)]_{(1-x)}\text{Se}_4$ is formed between Sm₃Se₄ and Sm₂Se₃ phases. Ln₃Se₄–Ln₂Se₃ solid solutions are formed for the following lanthanides: lanthanum, cerium, praseodymium, neodymium, and samarium [1, 13]. The differences between the unit cell parameters for Ln₃Se₄ and Ln₂Se₃ phases are: $\Delta a = 0.0003$ nm for lanthanum ($r\text{La}^{3+} 4f^0 5d^0 6s^0 = 0.103$ nm), $\Delta a = 0.0002$ nm for cerium ($r\text{Ce}^{3+} 4f^1 5d^0 6s^0 = 0.101$ nm); $\Delta a = 0.0009$ nm for praseodymium ($r\text{Pr}^{3+} 4f^2 5d^0 6s^0 = 0.099$ nm); and $\Delta a = 0.0008$ nm for neodymium ($r\text{Nd}^{3+} 4f^3 5d^0 6s^0 = 0.098$ nm).

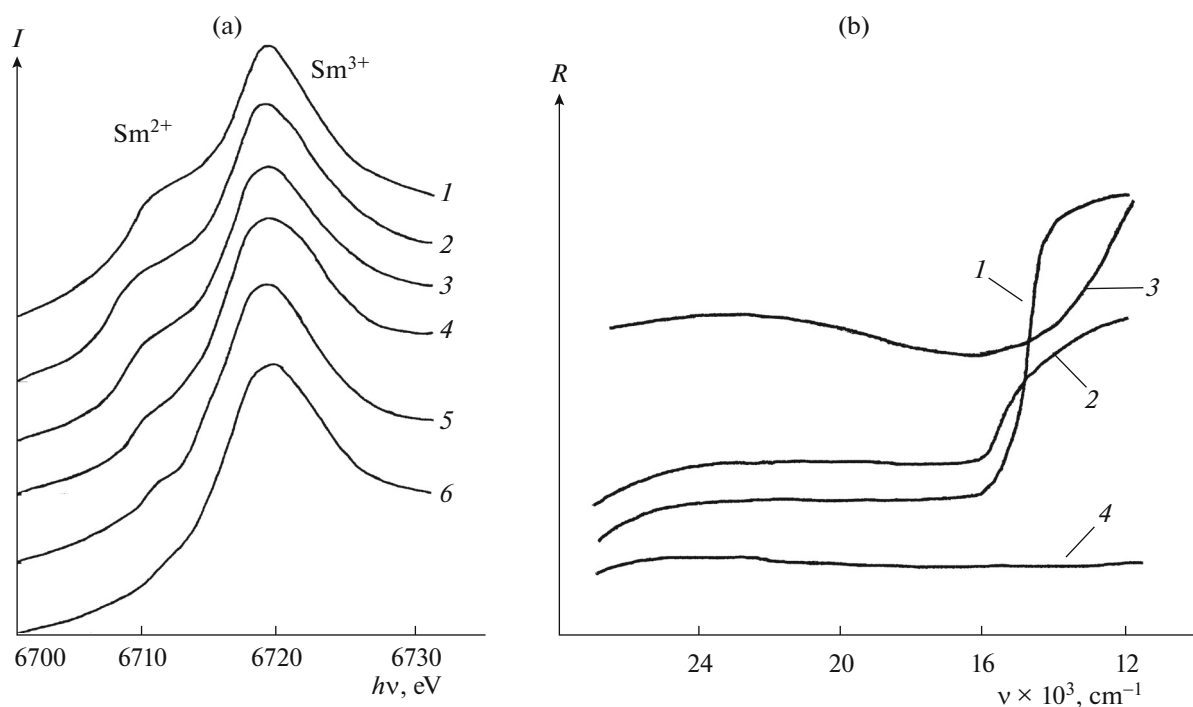


Fig. 4. Panel (a): L_{III} absorption spectra for samarium selenides: (1) $\text{SmSe}_{1.34}$, (2) $\text{SmSe}_{1.37}$, (3) $\text{SmSe}_{1.40}$, (4) $\text{SmSe}_{1.45}$, (5) $\text{SmSe}_{1.46}$, and (6) $\text{SmSe}_{1.48}$. Panel (b): Reflections from samarium selenide powders in the visible: (1) $\text{SmSe}_{1.48}$, (2) $\text{SmSe}_{1.45}$, (3) $\text{SmSe}_{1.40}$, and (4) $\text{SmSe}_{1.33}$.

In Sm_3Se_4 – Sm_2Se_3 solid solution ($r\text{Sm}^{2+} 4f^6 5d^0 6s^0 = 0.114 \text{ nm}$ [14]), the unit cell parameters change from 0.8924 to 0.8816 nm, $\Delta a = 0.0108 \text{ nm}$, which is one order of magnitude higher than for other cerium rare earths where they are stably trivalent. Valence state changes of samarium atoms in Sm_3Se_4 – Sm_2Se_3 solid solution were determined.

X-ray absorption spectra L_{III} (exposure time: 10^{-16} s [8]) feature two absorption peaks near 6713 and 6720 eV. The intensity ratio of these peaks is a measure of the Sm^{2+} and Sm^{3+} ion ratio (Fig. 4a). The Sm^{3+} percentage of the total Sm^{2+} and Sm^{3+} amount in the sample was derived from the plot with accuracy of $\pm 5\%$ (Table 1).

From experimental data, it flows that Sm^{2+} concentration steadily increases over the Sm_2Se_3 – Sm_3Se_4 extent, corresponding (within the error bar) to the Sm^{2+} percentage derived from the formula (as-batch) composition of the sample (Table 1). The solid solution should be formulated as $\text{Sm}_{1-x}^{2+}\text{Sm}_x^{3+}\text{Se}_{4-x}^{2-}$ ($x = 0-1$) and the composition of the Sm_3Se_4 phase as $\text{Sm}^{2+}\text{Sm}_2^{3+}\text{Se}_4$. Presumably, $4f$ -electron exchange between Sm^{2+} and Sm^{3+} occurs with a frequency of 10^{-14} s , as in Sm_3S_4 .

Experimentally determined Sm^{3+} percentages steadily exceed the calculated values by 2–4% (Table 1).

Table 1. Contents of Sm^{2+} and Sm^{3+} ions; characteristics of phases in Sm_3Se_4 – Sm_2Se_3 solid solution

Selenium content, at % Se	Samarium selenide	Unit cell parameter, nm	$\text{Sm}^{3+}/\text{Sm}_{\text{tot}}$, mol %		Reflection minimum ν_{min} , cm^{-1}	Bandgap width, ΔE , eV	$N/m^* \times 10^{21}$, cm^{-3}
			calcd.	measd.			
57.1	$\text{SmSe}_{1.34}$	0.8924	68	70	3000	–	0.265
57.8	$\text{SmSe}_{1.37}$	0.8880	72	76	900	–	0.024
58.4	$\text{SmSe}_{1.40}$	0.8875	77	82		1.95–1.86	
59.2	$\text{SmSe}_{1.45}$	0.8845	87	88		1.90–0.05	
60	$\text{SmSe}_{1.48}$	0.8816	95	>98		1.90–0.05	

Table 2. Eutectic composition in the Sm–SmSe system calculated by empirical equations [17]

Melting temperature, K, of			Empirical equations; eutectic composition, at % Se		
low-melting phase, Sm	high-melting phase, SmSe	eutectic	Efimov–Vozdvizhensky's	Cordes's	Vasiliev's
1345	2400	1300	2.2	3.7	2.2

Likely, surface samarium atoms in grains and samples are in the Sm³⁺ state due to, for example, the oxidation of Sm²⁺ to Sm³⁺ by oxygen.

Bandgap widths for Sm₂Se₃–Sm₃Se₄ solid solution samples were derived from the reflectivity (*R*) versus wavenumber (*v*) plot in the visible. The fundamental absorption edges of SmSe_{1.50} and SmSe_{1.45} samples coincide to within the determination error. For a SmSe_{1.40} sample, a diffused absorption edge is observed, making it difficult to determine the bandgap width ΔE . A likely reason for this is the transitions of electrons lying at localized levels inside the bandgap. Most likely, these are Sm²⁺ 4*f* electrons, which account to 22.8% in this sample. For SmSe_{1.37} and SmSe_{1.33} samples, the *R*(*v*) plot in the visible has no specific features in view of containing an even greater Sm²⁺ percentage. Additional light absorption by free carriers is also possible (Table 1). Samarium selenides from SmSe_{1.45} to SmSe_{1.48} are semiconductors with the bandgap $\Delta E = 1.90 \pm 0.05$ eV.

Between SmSe and Sm₃Se₄ phases, a eutectic is formed of composition 54.5 at % Se at (2100 ± 50) K. The eutectic morphology changes depending on the chemical composition of the sample. Polished samples of samples having compositions in the region where primary crystals of the Sm₃Se₄ phase are formed, clearly show primary Sm₃Se₄ grains as elongated ovals or polyhedra of 30 to 90 μm and the eutectic formed by alternating elongated crystals of SmSe and Sm₃Se₄ phases sized 3–7 μm on the average (Fig. 2). As their content increases in the region where SmSe primary crystals are formed, the content of the eutectic in the form of a mixture of SmSe and Sm₃Se₄ phase grains decreases. Oval grains of the SmSe phase are observed in microstructure images with Sm₃Se₄ phase grains mostly in between.

In samples with compositions systematically approaching the eutectic compositions, their SmSe and Sm₃Se₄ primary grains decrease in size and microhardness values (Fig. 3). The eutectic temperature was determined by VPTA in samples whose compositions approaches the eutectic composition. The enthalpy of melting for the Sm₃Se₄ phase, equal to 136 kJ/mol, was derived from the liquidus and solidus positions

from the eutectic to Sm₃Se₄ using the Van Laar equation [16].

In all samples from the range 0–50 at % Se, XRD and MSA detect only SmSe phases and metallic samarium. In 5, 10, and 25 at % Se samples, there are orange-colored oval SmSe grains sized 20–90 μm in the light field of metallic samarium with infrequent inclusions of SmSe fine grains sized 3–5 μm. In view of the high volatility of metallic samarium, VPTA was used to determine the eutectic temperature. The temperature at which a liquid phase appeared in Sm + SmSe samples was found to be 1300 ± 10 K against the melting point of metallic samarium (1345 K [4, 5]) (Fig. 1). The eutectic composition was calculated from empirical equations (Table 2) [17].

We have not managed to prepare a compact sample of eutectic composition. At 1200–1250 K, a noticeable part of metallic samarium was transferred to cold portions of an ampoule or reactor.

We took the eutectic composition to be 2.5 ± 1 at % Se and the eutectic melting temperature to be (1300 ± 10) K.

ACKNOWLEDGMENTS

This study was supported by the Russian Foundation for Basic Research (project no. 14-03-32062) and by Government Agreement no. 2014/228(1-14) (project no. 996).

REFERENCES

1. *Rare-Earth Chalcogenides*, Ed. by E. I. Yarembash and E. I. Eliseev (Nauka, Moscow, 1975) [in Russian].
2. T. Grundmeier and W. Urland, *Z. Anorg. Allg. Chem.* **621**, 1977 (1995).
3. O. V. Andreev, V. B. Kharitontsev, and A. V. Elyshev, *Russ. J. Inorg. Chem.* **58**, 910 (2013).
4. O. V. Andreev and V. B. Kharitontsev, *Vestn. Tyumensk. Gos. Univ.*, No. 5, 211 (2011).
5. V. B. Kharitontsev and P. O. Andreev, *Izv. Vyssh. Uchebn. Zaved., Khim. Khim. Tekhnol.* **55** (3), 46 (2012).
6. T. Yu. Shilkina, L. G. Gorbunova, and I. G. Vasil'eva, *Izv. Akad. Nauk SSSR, Neorg. Mater.* **23**, 1103 (1987).
7. N. Y. Pribil'skiy, J. G. Vasilieva, and R. S. Gamidov, *Mater. Res. Bull.*, No. 9, 1 (1982).

8. N. Yu. Pribyl'skaya, Candidate Dissertation in Chemistry (Tyumen', 1999).
9. O. V. Andreev, N. N. Parshukov, and V. M. Andreeva, *Zh. Neorg. Khim.* **39**, 6 (1994).
10. O. V. Andreev, N. N. Parshukov, A. V. Kertman, and T. M. Kislovskaya, *Russ. J. Inorg. Chem.* **41**, 284 (1996).
11. A. V. Golubkov, N. F. Kartenko, and V. M. Sergeeva, *Fiz. Tverd. Tela* **20**, 228 (1978).
12. G. Vaitheeswaran, V. Kanchana, S. Heathman, and M. Idiri, *Phys. Rev. B* **75**, 1 (2007).
13. V. F. Litvinenkj and A. R. Kopan, *Powder Metallurgy Metal. Ceram.* **47**, 466 (2008).
14. R. D. Shannon, *Acta Crystallogr., Sect. A* **32**, 751 (1976).
15. *Physics and Chemistry of Rare-Earth Elements. Handbook*, Ed. by K. Gshnaidner and L. Airing (Metallurgiya, Moscow, 1982) [in Russian].
16. N. A. Khritokhin, O. V. Andreev, E. A. Olennikov, and T. M. Burkhanova, *Russ. J. Inorg. Chem.* **47**, 123 (2002).
17. A. A. Ganeev, A. R. Khalikov, and R. R. Kabirov, *Vestn. UGARU* **11** (2(29)), 116 (2008).
18. A. A. Eliseev, G. M. Kuz'micheva, and Van Khuan, *Zh. Neorg. Khim.* **2**, 3167 (1976).

Translated by O. Fedorova